

3D earthquake ground motion simulations for the Christchurch area including the effects of the surface topography

Khurram S. Aslam,¹ Ricardo Taborda²

Corresponding author: Khurram Aslam, Centre for earthquake Research and information, University of Memphis, Memphis, Tennessee, USA. (ksaslam@memphis.edu)

¹Center for earthquake Research and information, University of Memphis, Memphis, Tennessee, USA.

²Department of Civil Engineering, EAFIT University, Medelln, Colombia.

Abstract.

We present initial results from a set of three-dimensional (3D) deterministic earthquake ground motion simulations for the northern Canterbury plains, Christchurch and the Banks Peninsula region, which explicitly incorporate the effects of the surface topography. The simulations are done using Hercules, an octree-based finite-element parallel software for solving 3D seismic wave propagation problems in heterogeneous media under kinematic faulting. We couple Hercules with the South Island Velocity Model (SIVM), which includes changes to the SIVM code in order to allow for single repetitive queries and thus achieve a seamless final-element meshing process within the end-to-end approach adopted in Hercules. We present our selection of the region of interest, which corresponds to an area of 120 km x 120 km, with the 3D model reaching a depth of about 60 km. Our simulation parameters are set to minimum shear wave velocity of 500 m/sec, and a maximum frequency of 2.0 Hz. To highlight the effects of topography, we compare the results of the 3D topographic model with respect to those of a flat (squashed) 3D model. We observe obvious differences between the velocity response of topographical model and flat model, specifically at locations of prominent topography. This suggests that topography is important to consider (in Ground motion prediction equations and ground motion simulations) for Christchurch area in order to get better estimates of the seismic hazard in the area.

1. Introduction

Central Canterbury area of New Zealand shows significant variation in topography over small distances in east-west direction. In the east of central Canterbury, the Banks Peninsula has variable elevation reaching ~ 900 m. Moving east to west, this variable topography converts to Canterbury plains which further changes to mountainous terrain reaching elevation of 1900 m in the west [Brown and Weeber, 1992; Forsyth et al., 2008]. The total east west relief of the region is about 2000 m. The Banks Peninsula on the east has mainly volcanic rocks of Cenozoic to Cretaceous age, the central plains has youngest sediments while the western part mainly has sedimentary rocks of early cretaceous to carboniferous age [Graham, 2008; Forsyth et al., 2008]. The topographic relief as well as the geological structure is highly heterogeneous in central Canterbury area. These two factors are important in terms of earthquake ground motions in an area since they can significantly change the ground motions during an earthquake. They can either reduce seismic risk of an area by damping ground motions or significantly increase seismic risk of an area by amplifying ground motions of an earthquake [Geli et al., 1988].

The Canterbury area has hosted a sequence of earthquakes at the start of this decade known as 2010 -2011 Canterbury earthquake sequence. Some of the earthquakes in this sequence caused extensive structural and geo-technical destruction in the region [Lee et al., 2017; Kaiser et al., 2012; Bradley et al., 2014]. Some previous Studies (e.g. [Bradley and Cubrinovski, 2011; Bradley, 2012]) have shown that one of the main factor enhancing the structural and/or geotechnical damage in the region, was the effect of three dimensional (3D) subsurface geologic structure of the area. This 3D subsurface geological structure

introduced basin edge and waveguide effects that amplified the ground motions significantly causing increased damage in the region. We believe that subsurface geological structure is not the only factor causing the main damage in the area. In addition to ground motion (GM) amplification due to subsurface geological structure, there may have been GM amplification due to wave-channeling and mountain edge effects associated with the significant variation of the topography in the region. Our study is mainly focused to investigate how the topographic variation of the central Canterbury region may have affected the surface ground motion of a moderate magnitude earthquake occurred in the same area.

Seismic wave amplification in the areas of high topographic relief is considered one of the main reasons of concentrated destruction during earthquakes. In the past, there have been many earthquakes during which damage due to high topographic relief is reported. These events included the 1909 Lambese earthquake [*Levret et al.*, 1988], 1976 Fruili earthquake [*Brambati et al.*, 1980], 1980 Irpinia earthquake [*Siro*, 1982], 1985 Chile earthquake [*Celebi*, 1987], 1994 Northridge earthquake [*Spudich et al.*, 1996; *Bouchon and Barker*, 1996; *Paolucci*, 2002], 1999 Athens earthquake [*Athanopoulos et al.*, 2001; *Paolucci*, 2002], 1986 Hualien earthquake [*Chiu and Huang*, 1992; *Lee et al.*, 2009], the 1989 Loma Prieta earthquake [*Hartzell et al.*, 1994] and the 1999 Chi-Chi earthquake [*Huang*, 2000].

Many studies has focused to understand the effects of topography on ground motions. Some of them used analytical aproach (e.g. [*Geli et al.*, 1988]) and some (e.g. [*Restrepo et al.*, 2016; *Komatitsch et al.*, 2004]) used numerical modeling to understand the effects of topography. *Restrepo et al.* [2016] studied the topographic effects of the Colombian Andes by including heterogeneities of topography of Aburra Valley, Antioquia in their

ground motion simulation studies. They ran four rupture scenarios of Magnitude 5 earthquake and using three model scenarios (realistic 3D velocity structure with topography, 3D velocity structure without topography, and homogeneous half-space with realistic topography). They showed that at some locations there was topographic amplification \sim as high as 500 percent while the locations within valley had a reduction in ground motions simulation about \sim 150 percent. *Komatitsch et al.* [2004] used spectral element approach to simulate Ground Motions in the Los Angeles Basin incorporating topography. *Stupazzini et al.* [2009] performed near-Fault Earthquake Ground-Motion Simulation in the Grenoble Valley, France using spectral element method. Their main emphasis was to study the effects of topographic variation of the area on the earthquake ground motions. *Lee et al.* [2009] performed Seismic Ground Motion simulation in the Yangminshan Region of Taiwan using Spectral-Element Method to study the topographic effects related to the area. They used a very high resolution digital elevation model (resolution \sim 1m). *Paolucci* [2002] performed ground motion simulation of many areas in Italy like Castellaro to observe the effect of topography.

We run earthquake ground motion simulations using physics based deterministic method with point source and realistic 3D velocity structure of the the Canterbury region, New Zealand. Our simulation domain comprises a $120 \text{ km} \times 120 \text{ km} \times 60 \text{ km}$ volume. We run our simulations with a max frequency of 2 Hz and min. shear wave velocity of 500 m/sec. We use finite element method code Hercules [*Tu et al.*, 2006] with topography implementation using a Virtual Topography scheme [*Restrepo and Bielak*, 2014]. The topography resolution used in our study is \sim 20 m. Our objective of this study is to examine the main differences of ground motion between two models i.e. flat model and topographic

model. We further observe the difference in ground motions in the same model by using two different attenuations i.e. elastic and inelastic. Our modeling study is performed to provide improved constraints on the effect of geomorphology of the Canterbury region on its seismic hazard.

2. Histotical and current seismicity of the Canterbury region

The area of Canterbury has hosted many damaging earthquakes in historical times. The 1869 earthquake of Magnitude 4.9 occurred near Christchurch City with an intensity measure of MM7 [Gledhill *et al.*, 2011]. The 1870 earthquake in the Selwyn District near Lake Ellesmere had an intensity measure of M7 [Gledhill *et al.*, 2011]. The 1888 earthquake of M 7.07.3 occurred in Amuri District, North Canterbury had a reported intensity of MM9 near epicentre. This earthquake had done much damage to buildings and numerous landslides and rockfalls were reported as a result of this earthquake [Cowan, 1991]. The 1901 earthquake with a magnitude of M 6.9 occurred in Cheviot, Hurunui District with a reported intensity of MM7. This earthquake caused liquefaction at Kaiapoi and lateral spreading [Pettinga *et al.*, 2001]. The 1922 earthquake of M 6.4 occurred at Motunau, Hurunui District with an intensity measure of MM7 Causing liquefaction in the areas of Pegasus Bay coast, Leithfield Beach and Waikuku [Pettinga *et al.*, 2001]. The 1929 earthquake of Mw 7.0 occurred in Arthur's Pass, Selwyn District [Doser *et al.*, 1999], The 1946 earthquake of ML6.2 at Lake Coleridge, Selwyn District had a minor structural damage to buildings and the Lake Coleridge hydro-electric power station. Numerous landslides and aftershocks were reported due to this earthquake [Downes, 1995]. The 1994 earthquake of Mw 6.7 Arthur's Pass, Selwyn District also did a considerable damage. Many landslides were mapped after this earthquake. A rockfalls blocked one of the main

state highway for almost a week. The Damage related to this earthquake was claimed more than US 3.2 million [*Abercrombie et al.*, 2000]. The 1995 earthquake of Mw 6.2 Cass, Selwyn District had an intensity measure of MM6 near epicentre. This earthquake was also a damaging earthquake [*Gledhill et al.*, 2000].

The area of christburgh gained serious attention after The 2010-2011 Canterbury earthquake sequence. The sequence started with September 2010 Darfield earthquake having a magnitude of 7.1 occuring about 40 km away from Christchurch. It was named Darfield since it occurred about 9 km away from the town of Darfield. The main fault movement was strike-slip [Brackley, 2012]. The earthquake was relatively shallow having a depth of 10.8 km. It occurred on a blind fault, the Greendale fault [*Gledhill et al.*, 2011]. The maximum horizontal displacement of Greendale fault was reported to be 5 m while the vertical displacement was reported 1.5m. The surface rutpute was reported 30 km [*Gledhill et al.*, 2011; *Quigley et al.*, 2012; *Potter et al.*, 2015]. There was a big aftershock sequence followed by the main event. Some strong Aftershocks included M 4.9 December 2010 earthquake. M 6.3 February 2011 earthquake, M 6.0 June 2011 earthquake and two earthquakes of Mw 5.8 and Mw 5.9 on December 2011. The 6.3 magnitude February event occurred beneath the Canterbury Plains having a very shallow depth (approx. \sim 5 km). This event also occured on a blind fault with accelerations reaching 2.2 g in some areas [*Kaiser et al.*, 2012]. Similar accelerations were recorded (close to 2g) for the June 2011 earthquake at some stations. Since Canterbury Plains are built as a result of sedimentation from rivers that flowed from Southern Alps and deposited post-glacial alluvial gravels [*Forsyth et al.*, 2008]. The Canterbury plains specially Christchurch city is highly vulnerable to liquefaction. This is what happened during 2010-2011 Canterbury

earthquake sequence and many Liquefaction sites were reported during these sequence which caused interruptions to the recovery effort carried out during those earthquakes.

3. Computational method of ground motion simulations

Models for the prediction of earthquake ground motions are constructed using two different approaches. One approach is mathematical where a model is based on physical principles and the second approach is experimental where more emphasis is given to fit the model with experimental data rather focusing on the physical insight of the model [Ólafsson *et al.*, 2001; Douglas and Aochi, 2008]. The methods using mathematical approach are mostly called Physics- based methods. Some of the commonly used physics based methods like Finite difference, Finite element and spectral element methods are deterministic methods. This current study utilizes HERCULES, a finite element method (FEM) simulation software for anelastic wave propagation developed by Quake Group at Carnegie Mellon University [Tu *et al.*, 2006; Taborda *et al.*, 2010] to get the ground motions of christchurch area.

3.1. FEM methodology

The deterministic physics based methods of ground motion simulation are based on solving the momentum equation that is given as:

$$\rho \ddot{u}_i = \sigma_{ij,j} + f_i \quad (1)$$

Here, double-dot above u denotes the second partial derivative with respect to time. The equation is written in Cartesian coordinates where u_i and f_i represent the displacement and the body forces in the i direction. The Cauchy stress tensor is given by σ_{ij} while $\sigma_{ij,j}$

is the space derivative of Cauchy stress tensor w.r.t to j direction and ρ is mass density. This stress tensor is related to the strain tensor ϵ_{pq} through a fourth order tensor as

$$\sigma_{ij,j} = C_{ijpq}\epsilon_{pq} \quad (2)$$

Using symmetry of stress and strain tensor, and assumption of isotropy within a rock, the Cauchy stress tensor can be written in terms of displacements and Lame parameters (λ and μ) as shown in (4)

$$C_{ijpq} = \lambda\delta_{ij}\delta_{pq} + \mu(\delta_{ip}\delta_{jq} + \delta_{iq}\delta_{jp}) \quad (3)$$

$$\sigma_{ij} = \lambda\delta_{ij}u_{k,k} + \mu(u_{i,j} + u_{j,i}) \quad (4)$$

As described earlier, all the FEM methods including HERCULES are based on solving equation (1) with Cauchy stress tensor given by (4). The final momentum equation is converted into weak form using standard Galerkin method and then problem is discretized in space. This procedure converts the momentum equation into a matrix form as

$$M\ddot{u} + Ku = f \quad (5)$$

Here M is systems mass matrix and K is the systems stiffness matrix, the term f on right hand side is the assembled vector of body forces. A detailed description of FEM method with forms of the matrices is provided by *Taborda and Rotenb* [2015].

3.2. Topographic implementation

The topographic implementation in Hercules is done using Virtual Topography approach [*Restrepo and Bielak, 2014*]. This approach consists of two steps. During the first step, the topography above a flat surface is accommodated using an unstructured mesh (cubic elements). In the second step, the cubic elements are subdivided into five tetrahedral elements and then the stiffness matrix of each of the tetrahedral element is scaled using the topographic volume present in this tetrahedron. One advantage of this topographic implementation is that it does not affect the time stepping or the efficiency of the numerical approach. A detailed description of virtual topographic implementation with benchmark problems are provided by *Restrepo and Bielak [2014]*.

4. Model for simulations

The first column in Fig. 3 (i.e. original workflow) shows a typical workflow performed during the ground motion simulation modeling. A domain size is selected before running a simulation and then simulation parameters are decided. Similarly, a source model, material model and topographic model are selected a-priori to run a ground motion simulation.

The details of each of these is provided below.

4.1. Domain size and simulation parameters

One of the important considerations in ground motion simulations is the selection of dimensions of simulation domain. This dimension is a main factor controlling the size of the problem that is solved during a simulation. Once the dimensions is selected, the next part is to select a source and material model with some definition of modeling parameters [*Taborda and Rotenb, 2015*]. We select a domain having a size of 120 km east-west, 120

km north-south, and 60 km in the depth direction for all of our simulations. We select this region so that we can cover the main topographic regions of the central Canterbury region i.e. peninsula region, plain region and high topographic region. Figure 1 shows the horizontal surface projection of the simulation domain in the South Island (left), and detailed inset of the simulation domain. The star indicates the epicenter location of the point source used in our simulations. We select a shear wave velocity of 500 m/sec and a max. wave frequency of 2 Hz in order to make the simulation less expensive. The outputs of the code are ground displacements, velocity, and accelerations at the provided coordinates of earth surface at any desired sampling frequency. We run our 3D ground motion simulations using elastic material properties and anelastic material properties. The anelastic model uses rayleigh damping to imply effects of anelasticity.

4.2. Source model

The package used in this study (Hercules) has capacity to handle both point source as well as extended fault source models. We have performed our simulations with a point source. The epicenter location of the point source has a latitude 43.50° S and a longitude of 172.80° E. The star in Fig. 1 indicates the epicenter location of the point source used in our simulations. It corresponds to an aftershock of the 2010-2011 Christchurch earthquake sequence, with a magnitude M_w 5.4. The triangles indicate the location of an artificial array of stations used for the analysis of results.

4.3. Material model

Canterbury subsurface geological structure has significantly influenced the surface ground motions in some of the past earthquakes. The sedimentary basins in the region

(e.g. Rakaia basin) and subsurface volcanic edifice has been the most dominant features in effecting the wave propagation and surface ground motions in the area [Bradley, 2012; Browne *et al.*, 2012]. Since we are running ground motion simulations of the Canterbury area to isolate the effects of surface topography from the subsurface geological structure effect of the region and the most importance consideration in running a 3D simulation is the selection of a realistic material model [Taborda and Rotenb, 2015], we consider finding a best possible velocity model of the region to be used in this study. There have been many studies (e.g., [Hicks, 1989; Jongens, 2011; Ghisetti and Sibson, 2012]) to investigate the subsurface geological structure of this area which helps defining a reasonable subsurface approximation of geological structure. A recent study Lee *et al.* [2017] combines the above mentioned studies with other data sets from different resources to construct a 3D velocity model of the region. This study has been successful to reach a very high resolution i.e. (~ 10 m) in some areas due to its utilization of direct field measurement data like seismic reflection data, well log data (from petroleum and water wells), and cone penetration test data. This study provides a detail velocity model of the region from the basement rock to all the geological rock surfaces overlying it in the region. We use the velocity model of Lee *et al.* [2017] to define a crustal material model in this study. We define the material model below Moho using different tomographic studies of the regions [ref]. Our implementation of the material model into Hercules is given in Fig. 9. We modify the original workflow of Hercules to perform a point base query at a given position into the material model of Canterbury as can be seen in the second column of Fig. 9. The shear wave velocity at the surface of our modeling domain can be seen in Fig. 2 (b).

4.4. Topographic model

The topographic model of the current modeling domain is constructed by combining New Zealand nationwide digital elevation model LIN and New Zealand bathymetry Koo contour data using ArcGIS ?. Our current resolution of the topographic model is 20 m. Figure 2(a) shows the relief of the modeling domain. The total relief of the modeling domain is ~ 3400 m.

5. Results and Discussion

Figure 4 shows the ground motion response for flat model along the artificial array of stations A-A' (shown in Fig. 1). The ground motions are a result of simulation runs with a maximum frequency of 1 Hz and a minimum velocity of 500 m/sec, and presents only the vertical component of velocity. The seismograms along the stations A-A' with flat model represents the propagation of the different seismic phases through different sub-surface geological structures of the considered region with no effect of topography. As expected, the direct P waves, which is the first phase in the seismograms, arrives first at the station closest from the epicenter (location marked with the star) and then it reaches to other station with some delay based on its epicentral distance (Fig. 4 (a)). The wavefield is significantly amplified for the stations present in the middle of the array which can also be seen at seismograms at the middle of Fig. 4(a). This amplification is expected based on the material model of the region as these stations are mainly from the 'plain region', a region dominated by unconsolidated sedimentary rocks and low velocity sediments. The material properties of the region has caused a significant amplification in the velocity response at those stations. Furthermore, the region of low velocity sedimentary cover has also caused resonance in the seismic signal. This resonance can be observed in the

signal as a longer duration of signal for stations in the middle of array as compared to the stations present at the region of high elevation (at the left of array AA') or the stations present at the bank of peninsula which are on the right side of array AA'. Fig. 4(b) shows the peak vertical velocity in the simulation with a flat model. The peak ground velocities are relatively lower (... cm/sec) in the mountain side and Bank of peninsula (cm/sec) while a high value of the seismic velocities (... cm/sec) is observed in the plain region having sedimentary cover. The region of high amplification is marked in Fig. 4(b) with an arrow and specifies the existence of low velocity sedimentary cover of the region.

Figure 5(a) shows the perturbation seismograms corresponding to the difference between velocity signals of the topography model simulation and those of the flat model simulation along the same profile A-A' shown in figure 1. Figure 5(b) shows the peak vertical perturbation velocities and Fig. 5(c) presents the elevation above sea level of the stations along profile A-A'. The difference in velocity seismograms are visible along the whole profile depicting the importance of than the simplified flat model. This also suggests that the topography of a region should only be neglected if the ground motion simulations are done for a region with no significant topographic variations. Figure 5(b) shows that the region of highest difference between the flat model and the topographic model is at the left and right portion of the profile A-A'. The middle region (plain region) does not show any significant effect of topography. Based on comparison of Fig. 5(b) and Fig. 5(c), we can clearly observe that the stations that are showing the highest perturbation between the flat model and the topographic model are those which have a higher elevation than the surrounding. This means that Fig. 5(b) and Fig. 5(c) are well correlated suggesting that the location present at higher elevations have a tendency to

receive more ground shaking and hence a higher seismic hazard as compared to a location with similar material properties but at zero elevation for a similar magnitude earthquake occurred at similar distance.

To observe in detail how the seismic signal is affected at each region (i.e. the topographic part in the west, the plain part in the center and the bank of peninsula part in the east) due to topography, we pick 4 different stations with contrasting topographic locations. The locations of these 4 stations is marked in Fig. 2 (a). Stations P1 and P2 are from the western mountain side, station P3 is from the central plain region and station P4 is from the Bank of peninsula region. The acceleration seismograms at each of these stations are plotted in Fig. 6. These acceleration seismograms are from a run performed with the maximum frequency of 2 Hz and minimum shear wave velocity of 500 m/s. Signals in red correspond to the flat model, whereas the blue signals are from the topography model. All signal are for the NS component of motion. As can be seen that station P1, P2 accelerograms are different for the topographic model and the flat model. The topography has caused an amplification of the ground motion at all of these stations. Similarly, the length of the later part of the signal has also been increased which shows effects of the reverberations and reflections happened solely due to presence of topography. Station P3 is placed in the region of Central Canterbury plain which does not show any signs of amplification or any increase in the length of signal. Station P4 also show some difference between accelerogram of flat and topographic model as the bank of peninsula region has considerable variation in its topography.

To learn how the amplitude response spectrum compares within both models (i.e. the flat model and the topographic model) for a station placed on a topographic location,

we plot the amplitude spectrum for station P1 for both flat model and model with topography (shown in Fig. 7). The spectrum for the case of flat model shows a uni-modal standard form, where the spectrum is flat at lower frequencies and has a decaying part at relatively higher frequencies. The spectrum for the case of topographic model is different from that of a flat model. This spectrum is bi-modal, showing two different peaks at different respective frequencies. This implies that there is a relatively higher probability of resonance and seismic hazard for the areas present at topographic relief and hence more consideration should be given it include the topography for running ground motion simulations. Furthermore, the flat model spectrum has smaller peak spectrum values as compared to the spectrum of the seismogram of the topographic model.

Fig. 8 shows the peak horizontal velocity at the earth surface as a result of simulations performed with a max. frequency of 1 Hz and a minimum shear velocity of 1000 m/sec. The extent of the figure is the same as our simulation domain. The top figures corresponds to peak horizontal velocity at the earth surface for flat model for elastic properties and anelastic properties while the Figs. on the bottom shows the same but for the case of topographic model. Fig 8(a) shows the case of elastic properties, with no topography, Fig. 8(b) shows anelastic case with no topography. Fig 8(c) shows elastic case with topography and Fig. 8(d) shows anelastic case with topography. Comparing Fig. 8(a) with 8(c) , we can clearly observe that the inclusion of the topography causes the amplification of the ground velocities as shown by red and darker colors in the north-west part of the figure where the area is mostly covered by mountainous terrain. This is not that obvious when comparing (b) with (d), since the elastic response may have reduced those motion. Comparing 8(a) with 8(b) or 8(c) with 8(d), we can clearly see that the elastic response

causes ground motions to be reduced. The region north of the peninsula has the highest ground motions mainly related to the sedimentary structure lying under that region. We can also observe some reduced ground motions at the south of Peninsula in the case of topographic model as compared to the flat model. The topographic relief is causing an increase in ground motions at the north-western part of the simulation domain (marked in fig. 8) while a decrease in the ground motions at the south-eastern part of simulation domain (marked in fig. 8). Figure 9 shows the comparison of anelastic model for a flat model and a topographic model at a max. frequency of 2 Hz and a minimum shear wave velocity of 500 m/sec. The anomalous region of peak velocity is now more prominent (with the increase of max. frequency and decrease of shear wave velocity). We can clearly see the amplification of the seismic velocities in the north-western part. We believe that increasing the max. frequency will show a more better amplification of the stations on the elevated region and will give more insights into the seismic signal and their amplitude response in areas of higher topographic variations.

6. Conclusion

We present initial results from an effort to generate earthquake ground motion synthetics for the Canterbury region using 3D simulation techniques considering the effects of the surface topography. We successfully coupled the QuakeCoRE South Island Velocity Model with Hercules and performed a set of simulations with increasing resolution in the maximum frequency and minimum shear wave velocity. Our comparisons of simulation results at max. frequency of both 1 and 2 Hz reveals that the effects of topography are prominent in the region of topographic variation. This suggests the need of including topography of those regions that have significant variations in topography, when the syn-

thetic ground motion simulations are performed. To quantitatively describe the effects of topography on ground motions, we will run similar simulations with an increased max. frequency(i.e. 4 Hz) and reduced min. shear wave velocity (i.e. 350 m/s).

Our results show a comparison between flat model and topographic model, as well as a comparison between the elastic model and the anelastic model. The comparisons have given us insights into how the earth surface in Christchurch area may respond to intermediate magnitude earthquakes under the given subsurface geological structure, and current surface topography. Although, all these models have differences in their physics and hence have differences in their output, but all these models suggest that topography is essential to consider into Ground motion prediction equations and ground motion simulations of Christchurch in order to get better estimates of seismic hazard of the area. Our future work is based on comparison of output of each model with real data observations.

Acknowledgments. We thank Quakecore Newzealand for providing the velocity model for the Christchurch region. We are grateful to university of Memphis for providing their high performance computing resources to run some of these simulations.

References

().

().

Abercrombie, R. E., T. Webb, R. Robinson, P. McGinty, J. Mori, and R. Beavan (2000), The enigma of the arthur's pass, new zealand, earthquake: 1. reconciling a variety of data for an unusual earthquake sequence, *Journal of Geophysical Research: Solid Earth*, 105(B7), 16,119–16,137.

Athanasiopoulos, G., P. Pelekis, and V. Xenaki (2001), Topography effects in the athens 1999 earthquake: the case of hotel dekelia.

Bouchon, M., and J. S. Barker (1996), Seismic response of a hill: the example of tarzana, california, *Bulletin of the Seismological Society of America*, 86(1A), 66–72.

Brackley, H. (2012), *Review of liquefaction hazard information in eastern Canterbury, including Christchurch City and parts of Selwyn, Waimakariri and Hurunui Districts*, Environment Canterbury Regional Council.

Bradley, B. (2012), Ground motions observed in the darfield and christchurch earthquakes and the importance of local site response effects, *New Zealand journal of geology and geophysics*, 55(3), 279–286.

Bradley, B. A., and M. Cubrinovski (2011), Near-source strong ground motions observed in the 22 february 2011 christchurch earthquake, *Seismological Research Letters*, 82(6), 853–865.

Bradley, B. A., M. C. Quigley, R. J. Van Dissen, and N. J. Litchfield (2014), Ground motion and seismic source aspects of the canterbury earthquake sequence, *Earthquake Spectra*, 30(1), 1–15.

Brambati, A., E. Faccioli, G. Carulli, F. Cucchi, R. Onofri, S. Stefanini, and F. Ulcigrai (1980), Studio di microzonazione sismica dell'area di tarcento (friuli), *CLUET, Trieste*.

Brown, L. J., and J. H. Weeber (1992), *Geology of the Christchurch urban area: Scale 1: 25,000*, Institute of Geological & Nuclear Sciences.

Browne, G., B. Field, D. Barrell, R. Jongens, K. Bassett, and R. Wood (2012), The geological setting of the darfield and christchurch earthquakes, *New Zealand Journal of Geology and Geophysics*, 55(3), 193–197.

- Celebi, M. (1987), Topographical and geological amplifications determined from strong-motion and aftershock records of the 3 march 1985 chile earthquake, *Bulletin of the Seismological Society of America*, 77(4), 1147–1167.
- Chiu, H.-C., and H.-C. Huang (1992), Effects of the canyon topography on ground motions at the feitsui damssite, *Bulletin of the Seismological Society of America*, 82(4), 1646–1660.
- Cowan, H. (1991), The north canterbury earthquake of september 1, 1888, *Journal of the Royal Society of New Zealand*, 21(1), 1–12.
- Doser, D. I., T. H. Webb, and D. E. Maunder (1999), Source parameters of large historical (1918–1962) earthquakes, south island, new zealand, *Geophysical Journal International*, 139(3), 769–794.
- Douglas, J., and H. Aochi (2008), A survey of techniques for predicting earthquake ground motions for engineering purposes, *Surveys in geophysics*, 29(3), 187–220.
- Downes, G. L. (1995), *Atlas of isoseismal maps of New Zealand earthquakes*, vol. 11, Institute of Geological & Nuclear Sciences Limited.
- Forsyth, P., D. Barrell, and R. Jongens (2008), Geology of the christchurch area, institute of geological & nuclear sciences 1: 250000 geological map 16, *Lower Hutt, New Zealand*.
- Geli, L., P.-Y. Bard, and B. Jullien (1988), The effect of topography on earthquake ground motion: a review and new results, *Bulletin of the Seismological Society of America*, 78(1), 42–63.
- Ghisetti, F., and R. Sibson (2012), Compressional reactivation of e–w inherited normal faults in the area of the 2010–2011 canterbury earthquake sequence, *New Zealand Journal of Geology and Geophysics*, 55(3), 177–184.

- Gledhill, K., R. Robinson, T. Webb, R. Abercrombie, J. Beavan, J. Cousins, and D. Eberhart-Phillips (2000), The mw 6.2 cass, new zealand, earthquake of 24 november 1995: Reverse faulting in a strike-slip region, *New Zealand Journal of Geology and Geophysics*, 43(2), 255–269.
- Gledhill, K., J. Ristau, M. Reyners, B. Fry, and C. Holden (2011), The darfield (canterbury, new zealand) m w 7.1 earthquake of september 2010: A preliminary seismological report, *Seismological Research Letters*, 82(3), 378–386.
- Graham, I. J. (2008), *A continent on the move: New Zealand geoscience into the 21st century*, Geological Society of New Zealand.
- Hartzell, S. H., D. L. Carver, and K. W. King (1994), Initial investigation of site and topographic effects at robinwood ridge, california, *Bulletin of the Seismological Society of America*, 84(5), 1336–1349.
- Hicks, S. (1989), *Structure of the Canterbury Plains, New Zealand, from gravity modelling*, Geophysics Division, Department of Scientific and Industrial Research.
- Huang, B.-S. (2000), Two-dimensional reconstruction of the surface ground motions of an earthquake: The september 21, 1999, chi-chi, taiwan earthquake, *Geophysical research letters*, 27(18), 3025–3028.
- Jongens, R. (2011), Contours for the base of quaternary sediments under the canterbury plains between the ashley and rakaia rivers, *GNS Science Consultancy Report*, 132, 17.
- Kaiser, A., et al. (2012), The mw 6.2 christchurch earthquake of february 2011: preliminary report, *New Zealand journal of geology and geophysics*, 55(1), 67–90.
- Komatitsch, D., Q. Liu, J. Tromp, P. Suss, C. Stidham, and J. H. Shaw (2004), Simulations of ground motion in the los angeles basin based upon the spectral-element method,

- Bulletin of the Seismological Society of America*, 94(1), 187–206.
- Lee, R. L., B. A. Bradley, F. C. Ghisetti, and E. M. Thomson (2017), Development of a 3d velocity model of the canterbury, new zealand, region for broadband ground-motion simulationdevelopment of a 3d velocity model of the canterbury, new zealand, region, *Bulletin of the Seismological Society of America*, 107(5), 2131–2150.
- Lee, S.-J., Y.-C. Chan, D. Komatitsch, B.-S. Huang, and J. Tromp (2009), Effects of realistic surface topography on seismic ground motion in the yangminshan region of taiwan based upon the spectral-element method and lidar dtm, *Bulletin of the Seismological Society of America*, 99(2A), 681–693.
- Levret, A., C. Loup, and X. Goula (1988), The provence earthquake of 11th june 1909 (france). a new assessment of near field effects, *Modern Approaches in Geophysics*, pp. 383–399.
- Ólafsson, S., S. Remseth, and R. Sigbjörnsson (2001), Stochastic models for simulation of strong ground motion in iceland, *Earthquake engineering & structural dynamics*, 30(9), 1305–1331.
- Paolucci, R. (2002), Amplification of earthquake ground motion by steep topographic irregularities, *Earthquake engineering & structural dynamics*, 31(10), 1831–1853.
- Pettinga, J. R., M. D. Yetton, R. J. Van Dissen, and G. Downes (2001), Earthquake source identification and characterisation for the canterbury region, south island, new zealand.
- Potter, S., J. Becker, D. Johnston, and K. Rossiter (2015), An overview of the impacts of the 2010-2011 canterbury earthquakes, *International Journal of Disaster Risk Reduction*, 14, 6–14.

- Quigley, M., et al. (2012), Surface rupture during the 2010 mw 7.1 darfield (canterbury) earthquake: Implications for fault rupture dynamics and seismic-hazard analysis, *Geology*, 40(1), 55–58.
- Restrepo, D., and J. Bielak (2014), Virtual topography: A fictitious domain approach for analyzing free-surface irregularities in large-scale earthquake ground motion simulation, *International Journal for Numerical Methods in Engineering*, 100(7), 504–533.
- Restrepo, D., J. Bielak, R. Serrano, J. Gómez, and J. Jaramillo (2016), Effects of realistic topography on the ground motion of the colombian andes—a case study at the aburrá valley, antioquia, *Geophysical Journal International*, 204(3), 1801–1816.
- Siro, L. (1982), Southern italy november 23, 1980 earthquake, in *Proceedings of the seventh European conference on earthquake engineering, Athens, Greece*, pp. 20–25.
- Spudich, P., M. Hellweg, and W. Lee (1996), Directional topographic site response at tarzana observed in aftershocks of the 1994 northridge, california, earthquake: implications for mainshock motions, *Bulletin of the Seismological Society of America*, 86(1B), S193–S208.
- Stupazzini, M., R. Paolucci, and H. Igel (2009), Near-fault earthquake ground-motion simulation in the grenoble valley by a high-performance spectral element code, *Bulletin of the Seismological Society of America*, 99(1), 286–301.
- Taborda, R., J. López, H. Karaoglu, J. Urbanic, and J. Bielak (2010), Speeding up finite element wave propagation for large-scale earthquake simulations.
- Tabordaa, R., and D. Rotenb (2015), Physics-based ground-motion simulation, *Encyclopedia of Earthquake Engineering*, Springer, Berlin, Heidelberg, pp. 1–33.

Tu, T., H. Yu, L. Ramirez-Guzman, J. Bielak, O. Ghattas, K.-L. Ma, and D. R. O'hallaron

(2006), From mesh generation to scientific visualization: An end-to-end approach to parallel supercomputing, in *Proceedings of the 2006 ACM/IEEE conference on Supercomputing*, p. 91, ACM.

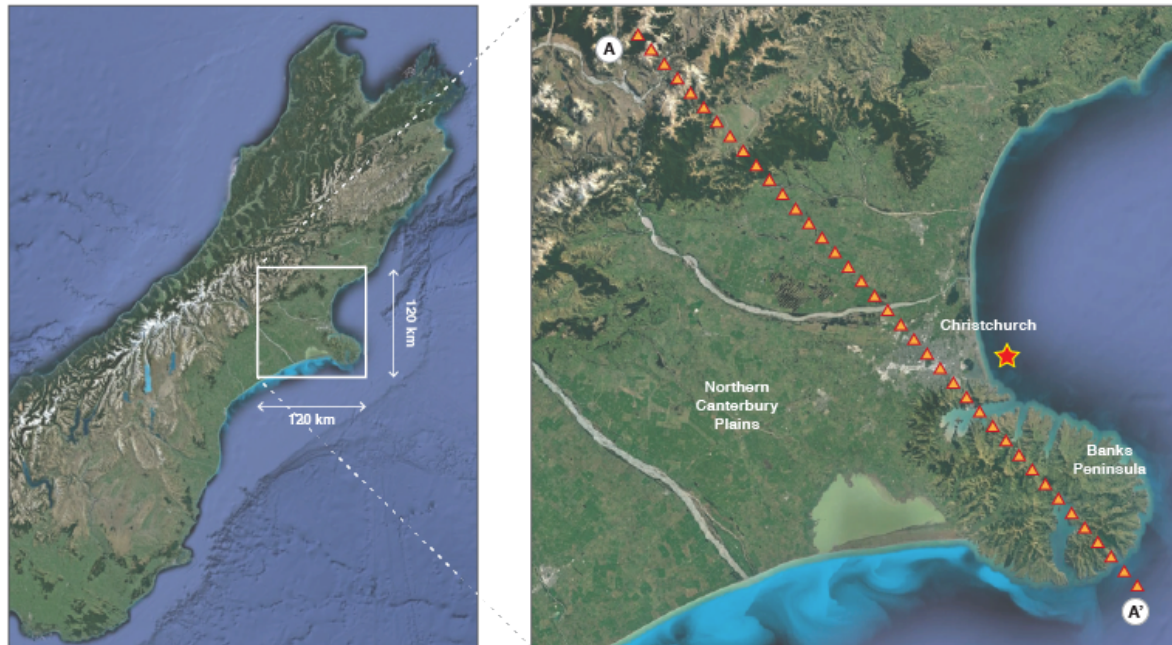


Figure 1. Horizontal surface projection of the simulation domain in the South Island (left), and detailed inset of the simulation domain. The star indicates the epicenter location of the point source used in our simulations. It corresponds to an aftershock of the 2010-2011 Christchurch earthquake sequence, with a magnitude M_w 5.7. The triangles indicate the location of an artificial array of stations used for the analysis of results.

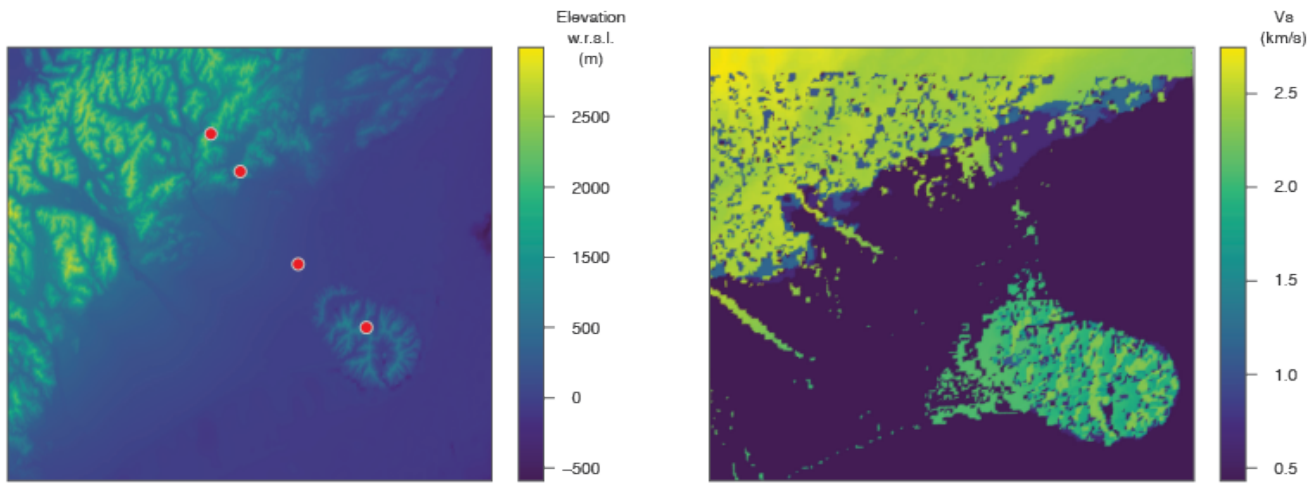


Figure 2. Surface topography and bathymetry of the region of interest (left), and surface shear wave velocity (V_s) for the same region, as obtained from the South Island Velocity Model (SIVM). The range of the relief in the region covered by the simulation domain is of 2,194 m, with a maximum elevation of 1,877 m and a maximum depth at sea of 317 m. In the simulations we consider minimum V_s values of 1,000 m/s for initial test runs, and 500 m/s for the final results. Red dots in the topography map indicate the location of a few stations of interest for later reference.

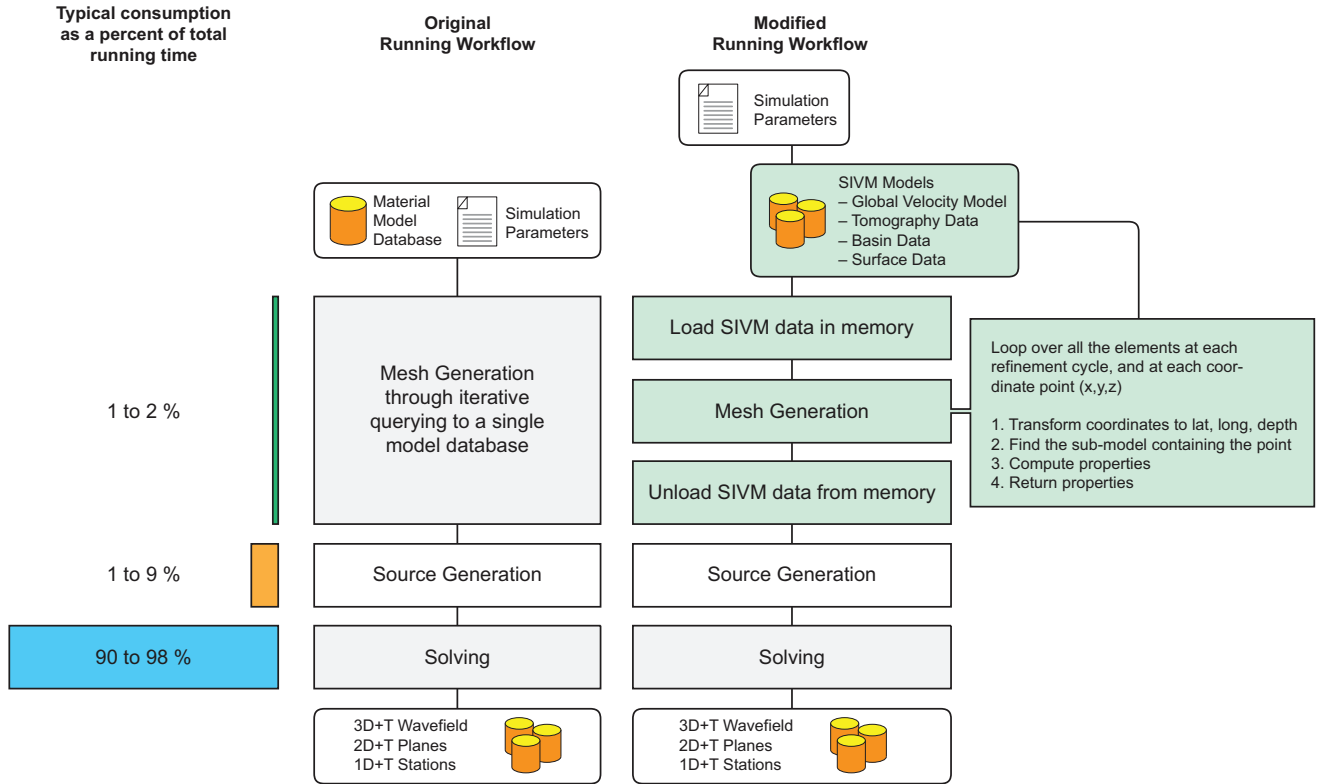


Figure 3. Simulation stages in Hercules. Left: typical running time-share for the three major computing operations. Center: original running workflow in which Hercules reads information from a single model database on disk during the meshing process. Right: modified running workflow coupling Hercules with the South Island Velocity Model.

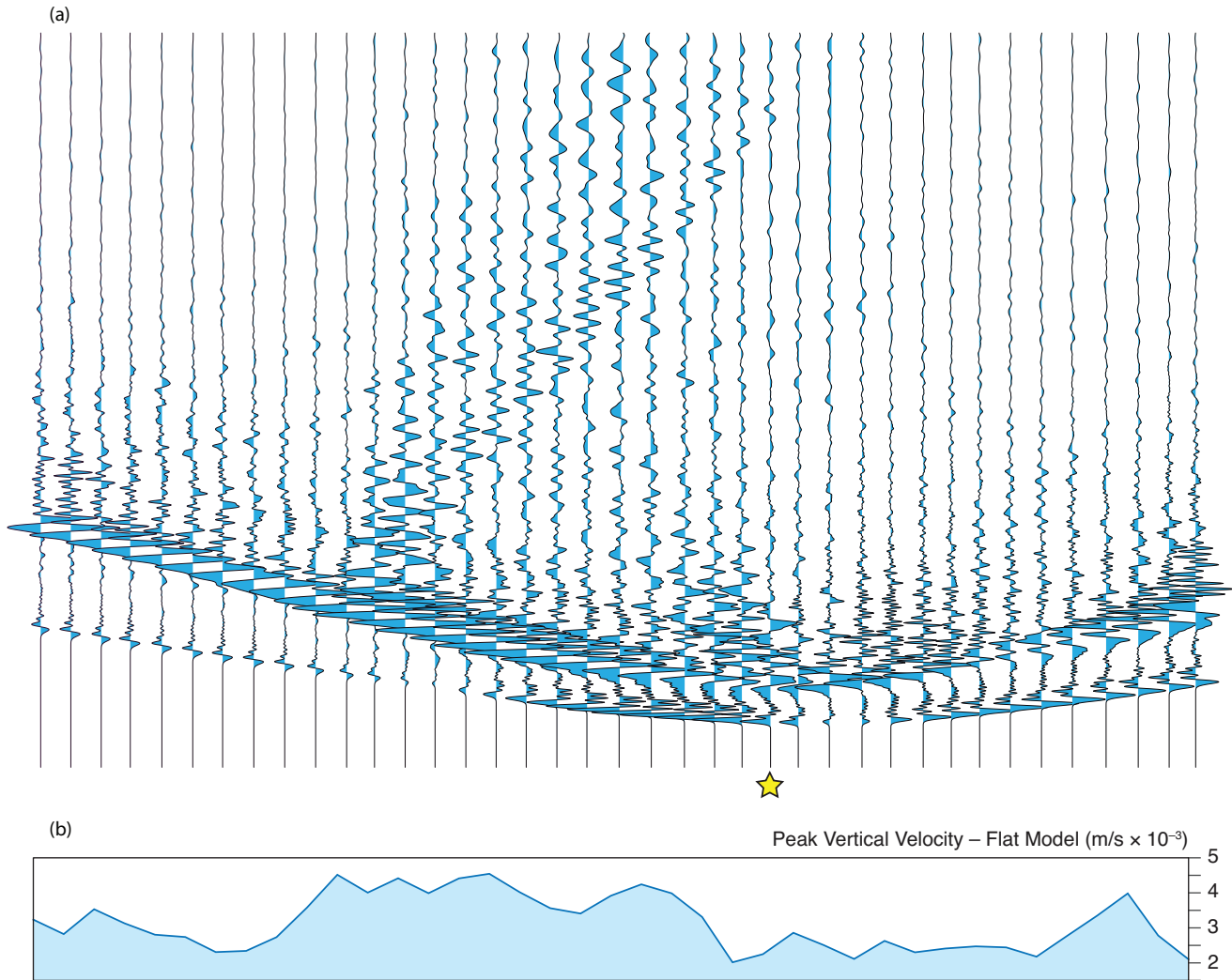


Figure 4. Peak ground response along the artificial array of stations A-A' shown in Fig. 1 for the flat model. The max. frequency of simulation is 1 Hz and the minimum shear wave velocity is 1,000 m/s. (a) Vertical velocity seismograms for the flat model. The first seismogram corresponds to the north western station of profile AA' while the last seismogram corresponds to the south eastern station of profile AA'. The seismograms in the middle corresponds to the plain area of Canterbury region. (b) peak vertical velocity in the simulation with a flat model. The peak velocities are relatively high for the stations from plainer region (middle portion). The subsurface geological structure causes an amplification to the wavefield which can be observed by the high values of peak vertical velocity for the middle stations.

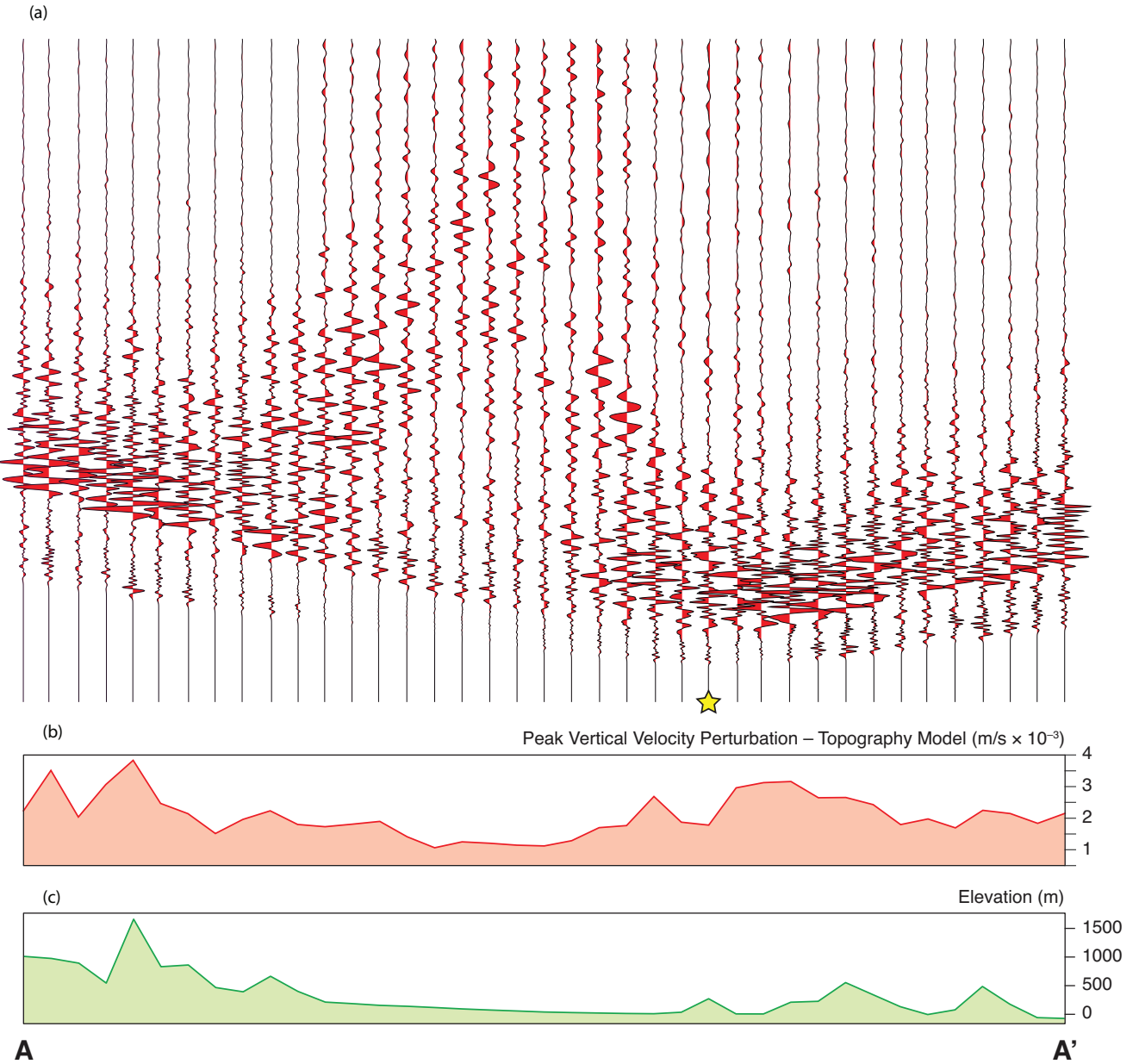


Figure 5. (a) perturbation seismograms corresponding to the difference between velocity signals of the topography model simulation and those of the flat model simulation (i.e. Fig. 4). (b) peak vertical perturbation velocities calculated from (a). The region of highest difference between the flat model and the topographic model is the left and right portion of the profile AA'. The middle portion (plain region) does not show any significant effect of topography. (c) Elevation above sea level of profile AA'. Based on comparison between (b) and (c), we can clearly observe that the stations that are showing the highest perturbation between the flat model and the topographic model are those which have a higher elevation than the surrounding.

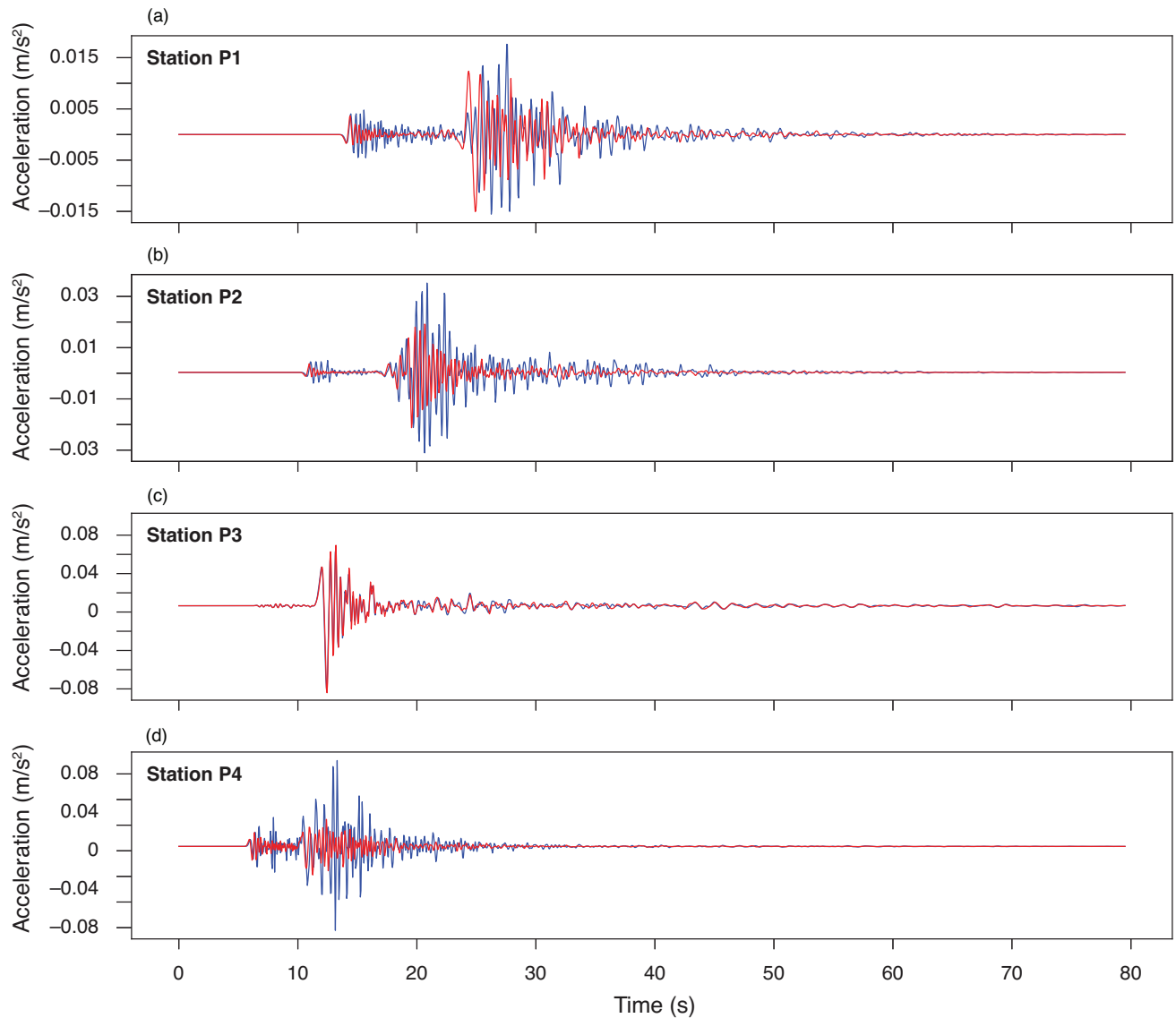


Figure 6. Acceleration seismograms from the 2 Hz and 500 m/s simulation at the location of the artificial stations P1 through P4 shown in Fig. 2. Signals in red correspond to the flat model, whereas the blue signals are from the topography model. (a) accelerogram from station P1, (b) accelerogram from station P2, (c) accelerogram from station P3, and (d) accelerogram from station P4.

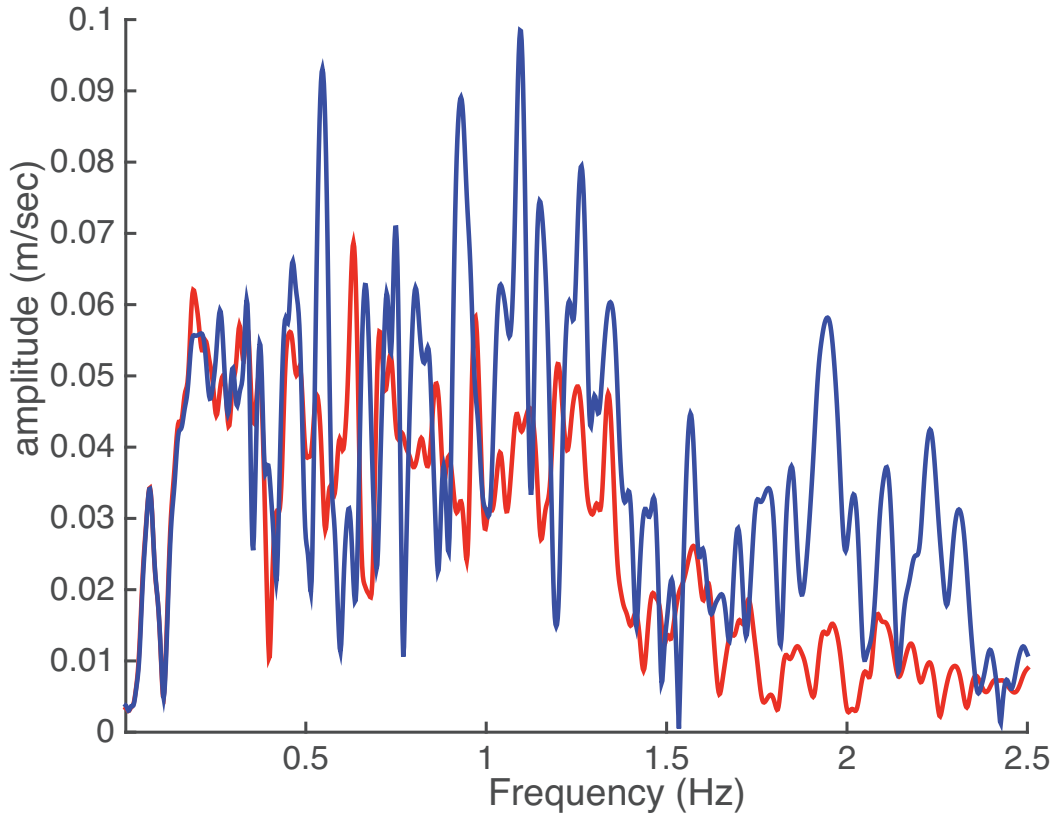


Figure 7. Amplitude spectra for the seismograms shown in Fig. 6(a). The red color spectrum is for the flat model and the blue color spectrum is for the topographic model. The flat model spectrum has lower peak values while the blue color spectrum has higher peak values.

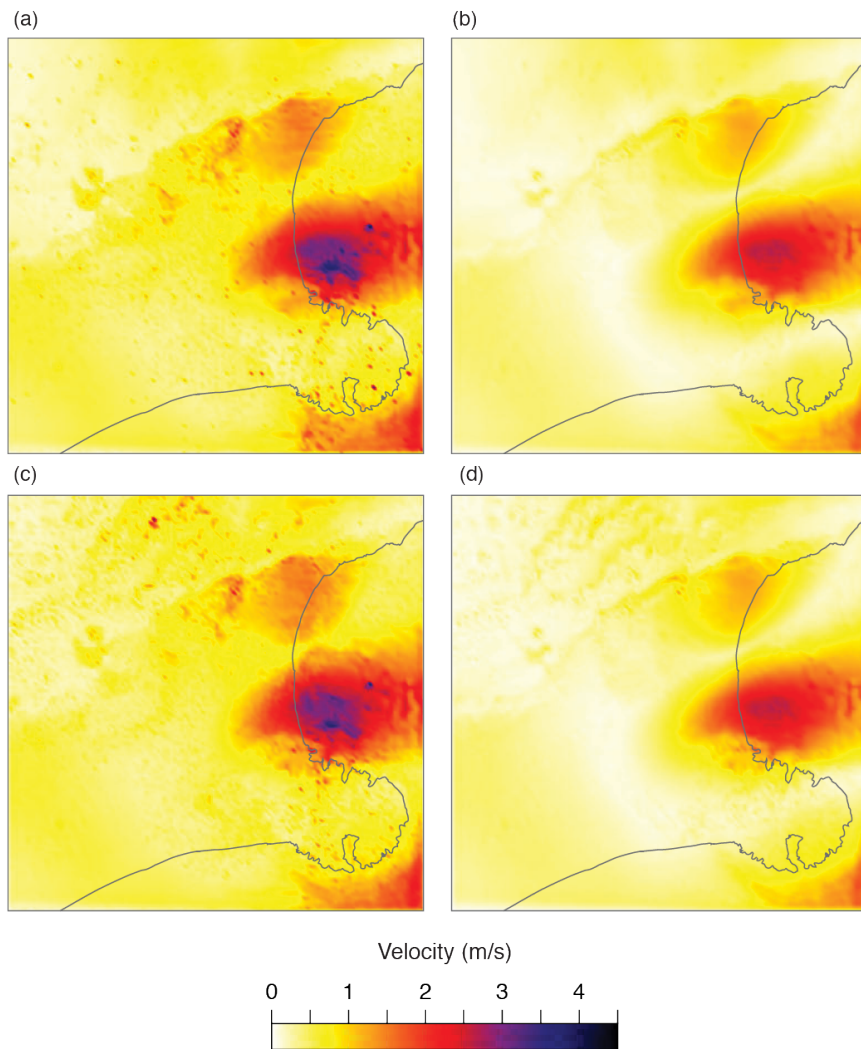


Figure 8. Results for simulations using different model for a max. frequency of 1 Hz and minimum shear wave velocity of 1000 m/sec. The color bar shows peak horizontal velocity. The models include with and without topography, and with and without attenuation (a) Elastic, without topography. (b) Anelastic, without topography. (c) Elastic, with topography. (d) Anelastic, with topography. we can clearly see that the inclusion of the topography causes the amplification of the ground velocities as shown by red and darker colors in the north-west part of the figure where the area is mostly covered by mountainous terrain. This is not that obvious when comparing (b) with (d), since the elastic response may have reduced those motion. The region north of the peninsula also has high ground motions mainly related to the sedimentary structure lying under that region. Furthermore, we can observe some reduced ground motions at the south of Peninsula in the case of topographic model as compared to the flat model.

March 14, 2019, 4:59pm

DOI: 10.1029/2018JB016473 | <https://doi.org/10.1029/2018JB016473>

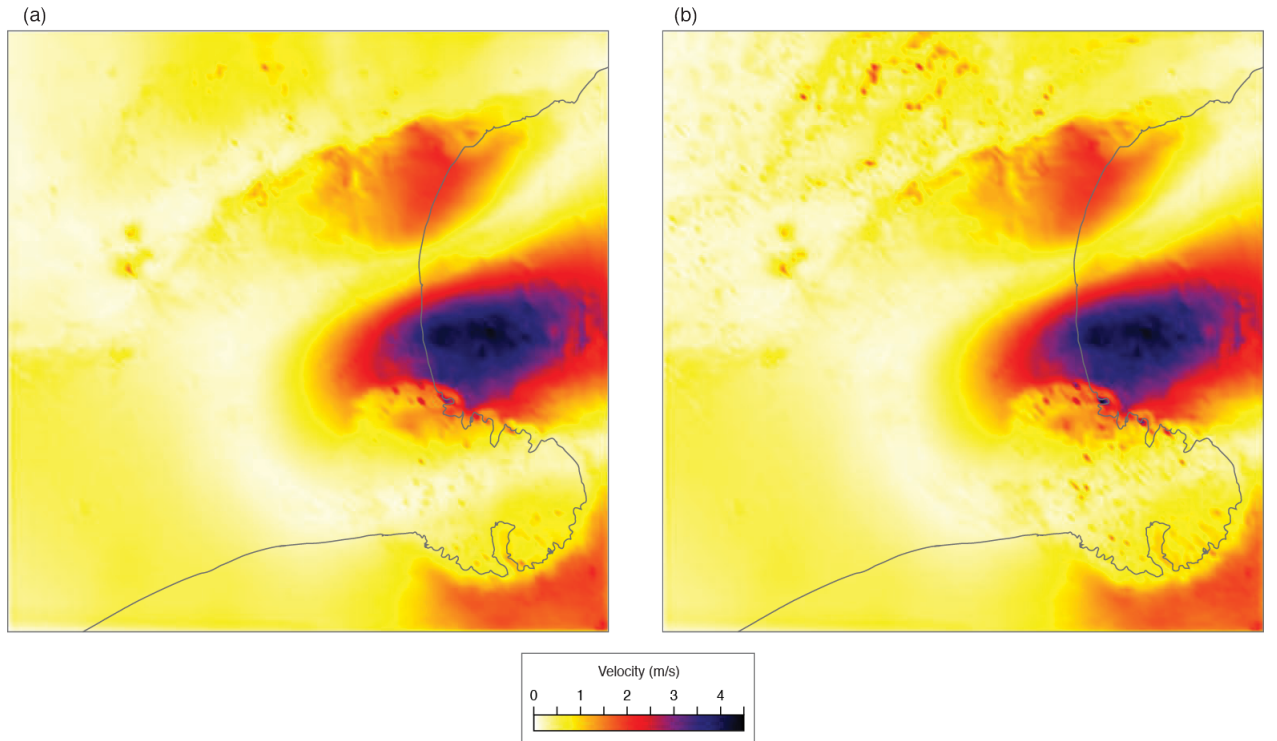


Figure 9. Peak horizontal velocity for a set of two simulations at a maximum frequency of 2 Hz and a minimum shear wave velocity of 500 m/s, both considering attenuation. (a) Flat model, (b) topography model. The anomalous region of peak velocity is relatively more prominent than with the increase of frequency and decrease of shear wave velocity.